Neurobiology of Disease 129 (2019) 29–37

Contents lists available at ScienceDirect

Neurobiology of Disease

journal homepage: www.elsevier.com/locate/ynbdi

Astrocyte transduction is required for rescue of behavioral phenotypes in the YAC128 mouse model with AAV-RNAi mediated HTT lowering therapeutics

Lisa M. Stanek*, Jie Bu, Lamya S. Shihabuddin

Sanofi Rare and Neurological Diseases, Framingham, MA, USA

ARTICLE INFO

Keywords:
Huntington's disease
Astrocytes
Adeno associated viral vectors
Striatum
Mouse model

ABSTRACT

Huntington's disease (HD) is a fatal autosomal dominant neurodegenerative disease caused by a CAG expansion, which translates into an elongated polyglutamine (polyQ) repeat near the amino-terminus of the huntingtin protein (HTT). This results in production of a toxic mutant huntingtin protein (mHTT) that leads to neuronal dysfunction and death. Currently, no disease-modifying treatments are available; however, numerous therapeutic strategies aimed at lowering HTT levels in the brain are under development. To date, studies have not closely examined the contribution of mHTT in neurons vs astrocytes to disease pathophysiology. To better understand the role of astrocytes in HD pathophysiology and the need for cell type specific targeting of HTT lowering therapeutic strategies, AAV capsids were employed that selectively transduce neurons, or both neurons and astrocytes. These vectors carrying miRNA sequences directed against HTT were injected into the YAC128 mouse model of HD to selectively lower HTT expression in neurons alone versus neurons and astrocytes. The results suggested that HTT lowering in neurons alone was not sufficient to rescue the motor phenotype in YAC128 mice. Furthermore, HTT lowering in both cell types was required to achieve maximal functional benefit. The study suggested that astrocyte dysfunction may play a critical role in HD pathogenesis, and thus astrocytes represent an important therapeutic target.

1. Introduction

Huntington's disease (HD) is a genetic neurological disorder caused by a CAG expansion in the gene encoding the huntingtin protein (HTT) (Ross, 2002; Walker, 2007; Ross and Tabrizi, 2011; Tabrizi et al., 2011; Wild and Tabrizi, 2017). Currently, no disease modifying treatments are available. However, numerous therapeutic strategies aimed at lowering HTT expression in the brain are under development (Kordasiewicz et al., 2012; Venuto et al., 2012; Stanek et al., 2013; Aronin and DiFiglia, 2014; Stanek et al., 2014; Miniarikova et al., 2017; Wild and Tabrizi, 2017). It still remains unknown whether HTT lowering in neurons is sufficient or whether targeting astrocytes is necessary for optimal therapeutic benefit. The HTT protein is found in both neuronal and non-neuronal cells throughout the brain; however, neurodegeneration is most prominent in striatal medium spiny neurons (MSNs) and cortical pyramidal neurons (Cudkowicz and Kowall, 1990; Vonsattel and DiFiglia, 1998). Medium spiny projection neurons (MSNs), the principal neurons of the striatum, show striking degeneration in HD patients, and have therefore been the primary focus of research so far (Nana et al., 2014). While it is clear that mHTT accumulation in MSNs plays a role in their atrophy and death, there is accumulating evidence that glial cells, astrocytes in particular, play a key role in the disease (Bradford et al., 2009; Bradford et al., 2010; Acuña et al., 2013; Tong et al., 2014; Benraiss et al., 2016; Khakh et al., 2017).

Astrocytes are the most abundant cell type in the brain, and are responsible for modulating synaptic transmission and providing metabolic support to neurons (Belanger et al., 2011). Brains from HD mouse and monkey models as well as HD patients show mHTT accumulation in glial cells (Hebb et al., 1999; Maragakis and Rothstein, 2001; Lobsiger and Cleveland, 2007; Wang et al., 2008; Bradford et al., 2009). Moreover, astrocytes expressing mHTT are unable to protect neurons against glutamate- or *N*-methyl-D-aspartate (NMDA)-induced toxicity in vitro, and are toxic to wild type neurons (Shin et al., 2005). In addition, striatal astrocytes from HD mouse models exhibit reduced capacity to buffer extracellular potassium, which may contribute to perturbed glutamate homeostasis and excitotoxic neuronal death (Khakh and Sofroniew, 2014; Tong et al., 2014; Jiang et al., 2016; Khakh et al., 2017). Brains from R6/2 HD mice show compromised metabolism and regulation of glutamate-GABA-glutamine cycling in astrocytes, resulting in impaired release of glutamine and GABA synthesis (Skotte et al., 2018). Interestingly, neuronal metabolism and neurotransmitter

* Corresponding author at: Sanofi, 49 New York Avenue, Framingham, MA 01701, USA.
E-mail address: lisa.stanek@sanofi.com (L.M. Stanek).

https://doi.org/10.1016/j.nbd.2019.04.015
Received 20 November 2018; Received in revised form 14 March 2019; Accepted 24 April 2019
Available online 28 April 2019
0969-9961/

dynamics were largely unaffected in this model, further suggesting that astrocytes may be central drivers behind HD pathology (Skotte et al., 2018).

HD mouse models, where mHTT is expressed exclusively in astrocytes, provide additional evidence for the key role of glial mHTT in HD neuropathology. HD transgenic mice, which express expanded huntingtin (160Q) under control of the glial fibrillary acidic protein (GFAP) promoter, exhibit age-dependent neurological phenotypes such as body weight loss and motor function deficits, and die earlier than wild-type or control transgenic mice (Bradford et al., 2009). This suggests that expression of mHTT in astrocytes alone is sufficient to cause neurological deficits. Mutant HTT was expressed in both astrocytes and neurons by the mating of GFAP-HD mice with N171-82Q mice (which express mHTT primarily in neuronal cells). The resultant double transgenic mice displayed more severe neurological symptoms and earlier death compared with N171-82Q mice that express mHTT in neurons alone (Bradford et al., 2010). Thus, mHTT-induced changes in neurons and astrocytes can synergize to cause HD pathology.

Similarly, using AAV viral vectors with cell type specific promoters driving mHTT expression, it was demonstrated that mice which expressed mHTT in both astrocytes and neurons exhibited the most severe behavioral alterations (Meunier et al., 2016). Recently, it was shown that reduction of mHTT in astrocytes, using a conditional BACHD mouse with floxed-m*HTT* and a GFAP-CreER^{T2} transgene, significantly reduced total mHTT burden in the brain and slowed progression of HD-relevant phenotypes in this mouse model (Wood et al., 2018). Furthermore, reducing mHTT in astrocytes led to a redistribution of mHTT aggregates in neurons, restored level of synaptic marker proteins, and reverses the electrophysiological abnormalities in excitatory transmission at corticostriatal synapses. Together, these data point to the potential of modulating mHTT in astrocytes in order to achieve enhanced neuronal function and neuroprotection and highlight the potential synergistic role of glial cells in HD pathophysiological mechanisms.

A number of therapeutic approaches are currently under development to directly target mHTT expression at the RNA level (siRNA, ASOs, Zinc fingers) or at the DNA level (CRISPR-mediated gene editing) (Malankhanova et al., 2017; Yan et al., 2018). Viral vectors are being optimized to deliver some of these HTT-lowering molecules to the brain (Gray et al., 2010; Hadaczek et al., 2016; Merienne et al., 2017; Miniarikova et al., 2017). Many of these approaches ameliorate disease phenotypes and pathology in HD rodent models and are moving towards clinical application (Boudreau et al., 2009; McBride et al., 2011; Kordasiewicz et al., 2012; Monteys et al., 2014; Stanek et al., 2014; Keiser et al., 2016; Miniarikova et al., 2017). The ability to target the cell types and brain circuitries most relevant to HD pathogenesis is critical to the success of these approaches. Therefore, a greater understanding of the necessity to target both neurons and astrocytes will be critical for maximally efficacious therapeutics for HD.

To better understand the relative contributions of astrocytes and neurons in HD pathophysiology, AAV-miRNA vectors of two different serotypes were utilized to lower HTT levels in either neurons alone, or both neurons and glia in the YAC128 transgenic mouse model, which recapitulates both behavioral and neuropathological features of HD (Slow et al., 2003; Van Raamsdonk et al., 2005). Using a novel AAV2 capsid (AAV2-HBKO) that produces widespread neuron-specific transduction in the brain (Sullivan et al., 2018), resulted in HTT lowering in neurons alone that was not sufficient to fully rescue the motor phenotype in YAC128 mice. In contrast, an AAV1 capsid that transduces both neurons and astrocytes completely rescued both motor and psychiatric phenotypes in these mice. Interestingly, HTT lowering in neurons alone with AAV2-HBKO rescued the psychiatric phenotype in the YAC128 mice, suggesting that different aspects of the total HD phenotype are determined by the complex interplay among different cell types.

2. Results

2.1. AAV1 and AAV2-HBKO vectors confer robust and widespread transduction following intrastriatal delivery

To evaluate the impact of neuronal versus neuronal and astrocytic expression of HTT lowering agents two vector serotypes were selected with different tropism (neurons versus neurons plus astrocytes) but similar expression patterns following intrastriatal delivery. AAV2 is a widely used serotype for selective neuronal transduction however its expression is highly restricted to the site of injection, likely due to its binding of heparan-sulfate proteoglycans (HSP) on the cell surface (Arnett et al., 2013). A modified AAV2 capsid unable to bind heparin, referred to as AAV2-HBKO (heparin binding knock out), was generated through site-directed mutations. AAV2-HBKO is capable of widespread transduction while maintaining strict neuronal tropism (Sullivan et al., 2018). In order to confirm the distribution of these two capsids following CNS delivery in YAC128 mice expression of enhanced green fluorescent protein (eGFP) was examined following injection of either AAV1-eGFP or AAV2-HBKO-eGFP into the striatum. Adult mice received bilateral intra-striatal injections of AAV1-eGFP ($N = 4$) or AAV2-HBKO-eGFP ($N = 4$). Brains were analyzed 4 weeks post-injection by confocal microscopy. Analysis of eGFP expression demonstrated that both AAV1-eGFP and AAV2-HBKO-eGFP vectors produced widespread expression of eGFP throughout the striatum (injection site) as well as adjacent cortical regions (Fig. 1A). Both AAV1 and AAV2-HBKO generated robust widespread GFP expression in subcortical regions including striatum, thalamus, hippocampus, as well as subthalamic nuclei and substantia nigra. Both vectors exhibited strong expression in cortical regions, with AAV2-HBKO expression distributed evenly across all cortical layers and AAV1 expression more prominently expressed in layers IV and V (Fig. 1A). Less GFP expression was observed in hindbrain regions such as medulla and cerebellum with both capsids, however AAV2-HBKO appeared to produce slight higher levels of hindbrain expression compared to AAV1 (Table 1). While these two vector serotypes generated similar levels of GFP expression and patterns of distribution in the brain there were notable differences in cellular tropism. In AAV2-HBKO-injected brains a majority (if not all) of the cells that expressed GFP exhibited neuronal morphology. In contrast, cells with both neuronal and glial morphology appeared transduced in AAV1 injected brains. Double labeling for astrocytic (GFAP) or neuronal (NeuN) markers confirmed that AAV2-HBKO exclusively transduced neuronal cells throughout the brain with minimal transduction of astrocytes (if any) while AAV1 transduced both neurons and astrocytes (Fig. 1B,C). We also examined whether AAV1 or AAV2-HBKO was capable of transducing microglial cells or oligodendrocytes by double labeling for a microglia/macrophage-specific calcium-binding protein, ionized calcium binding adaptor molecule 1 (Iba1) and oligodendrocyte transcription factor 2 (olig2). Consisted with our previous findings and the reported literature on the tropism of AAV1 and AAV2, we did not observe any double labeling in Iba1 positive or Olig2 positive cells, suggesting that neither serotype was capable of transducing these cell types (Fig. 1B,C bottom panels).

Quantification of the co-labeled images was performed to determine the percent neuron and astrocyte transduction in the striatum and cortex. AAV1 transduced both neurons and astrocytes in both the striatum (with a slight preference for neurons) and the cortex (Fig. 1D). It is interesting to note that a higher percentage of neurons were transduced at the injection site (striatum) when compared to astrocytes, while a larger percentage of astrocytes were transduced the more distal regions such as the cortex (Fig. 1D). This is consistent with our previously published findings in the nonhuman primate brain following AAV1-eGFP injection into the striatum (Hadaczek et al., 2016; Naidoo

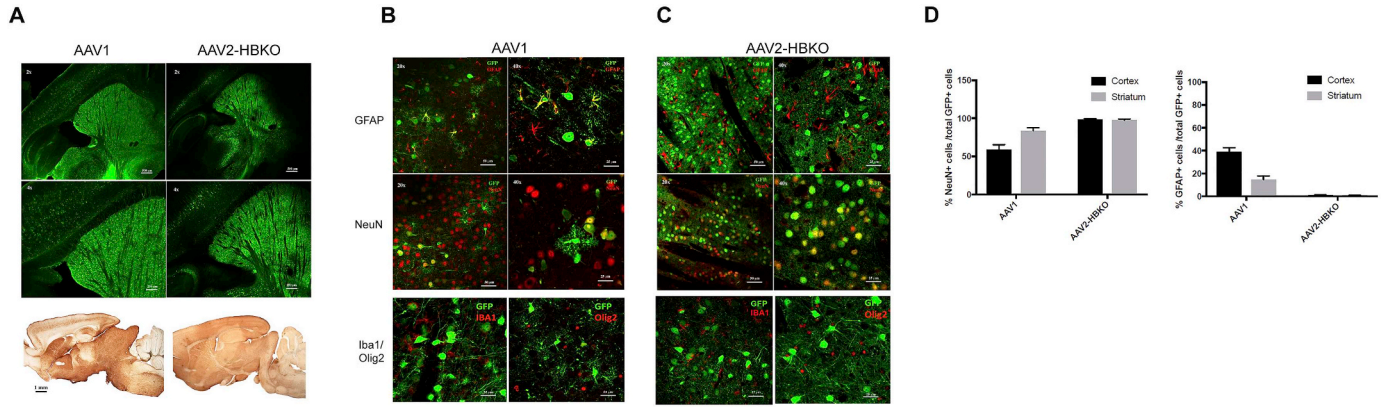

Fig. 1. AAV1-eGFP and AAV2-HBKO-eGFP distribution in the YAC128 mouse brain. (A) Representative images of eGFP transgene expression in the brains of YAC128 mice one month after intrastriatal injection of AAV1-eGFP (5×10^{12} VG/ml) ($N = 4$) or AAV2-HBKO-eGFP vector (2.2×10^{12} VG/ml) ($N = 4$). GFP expression was visualized with confocal fluorescence microscopy at 2x and 4x magnification and bright field microscopy at 1x magnification. (B,C) Neuronal nuclei (NeuN), glial fibrillary acidic protein (GFAP), ionized calcium binding adaptor molecule 1 (Iba1), oligodendrocyte transcription factor 2 (Olig2), and green fluorescent protein (GFP) immunohistochemical staining of sections from YAC128 mice treated with AAV1-eGFP (B) or AAV2-HBKO-eGFP (B) vector. All photographs were exposure-matched for accurate comparisons. Images are merged photos of representative striatal areas stained with immunofluorescence for NeuN (red), GFAP (red), Iba1 (red), Olig2 (red) and GFP (green) from mice that received an intrastriatal injection of AAV1-eGFP or AAV2-HBKO-eGFP. Scale bar = 50 and 25 μm as labeled. (D) Cell quantification of percent neuronal and glial transduction in the striatum and frontal cortex. (For interpretation of the references to colour in this figure legend, the reader is referred to the web version of this article.)

et al., 2018). AAV2-HBKO exclusively transduced neurons in both the striatum and cortex with no co-labeling of astrocytes observed in either region (Fig. 1D).

2.2. AAV1 and AAV2-HBKO-miRNA-HTT injection into the striatum of YAC128 mice results in equivalent levels of HTT reduction

To evaluate the efficacy of AAV1 and AAV2-HBKO vector mediated HTT reduction on HD phenotypes in YAC128 mice, AAV vectors designed to express a HTT lowering miRNA sequence under the transcriptional control of the chicken β-actin (CBA) promoter were generated. The ability of both AAV1- and AAV2-HBKO-eGFP-miRNA HTT vectors to drive expression of a miRNA and silence HTT expression in the striatum of YAC128 mice was examined. Adult mice received bilateral intra-striatal injections of AAV1-eGFP-miRNA-HTT ($N = 6$) or AAV2-HBKO-eGFP-miRNA-HTT ($N = 6$), and brains were analyzed 1 month post-injection using both qPCR and western blot. Control YAC128 mice were untreated and did not receive injections ($N = 6$). QPCR analysis revealed that levels of mutant human HTT mRNA in the striatum were significantly reduced by 45% in both the AAV1 and AAV2-HBKO injected brains when compared to untreated controls (Fig. 2A). Protein analysis by western blot indicated a commensurate reduction in HTT protein levels was also attained (40% reduction by AAV1 and AAV2-HBKO) (Fig. 2B) (Analysis of variance, one-way ANOVA; $^*p < .05$).

2.3. AAV1-miRNA-HTT but not AAV2-HBKO-miRNA-HTT improves motor deficits in YAC128 mice

The impact of AAV-mediated HTT reduction on the well-characterized motor and psychiatric deficits of the YAC128 HD mouse model was examined. For these studies the eGFP transgene was removed from the AAV vector constructs to eliminate confounds of GFP immunogenicity on the interpretation of behavioral data. Age-matched (2.5 month-old) YAC128 and wild-type (WT) littermate mice received baseline Rotarod testing in order to sort mice into equally matched treatment groups based on their Rotarod performance. The following week mice received bilateral intra-striatal injections of AAV1-miRNA-HTT ($N = 12$), AAV2-HBKO-miRNA-HTT ($N = 12$) or the AAV1-CTL control vector ($N = 12$), which contained a non-targeting control miRNA. One, two, and three months following stereotaxic surgery mice received Rotarod testing. One week following the last Rotarod test mice were assessed on the Porsolt Swim Test, sacrificed, and brain tissue was harvested for biochemical and histological assessments (Fig. 3A). Over the course of the study AAV1-CTL-treated YAC128 mice developed a progressive functional impairment in Rotarod performance, relative to their baseline performance that was significantly different from WT mice at each time point examined (two-way ANOVA with repeated measures; significant effect of treatment and time point; $p < .05$, * indicates YAC-AAV-CTL and AAV-HBKO were significantly different than WT at 3 mo. post injection; $p < .05$) (Fig. 3B). Consistent with our previous reports, by three months post injection YAC128 mice that had been treated with AAV1-miRNA-HTT performed significantly better than AAV1-CTL-treated YAC128 mice (# indicates YAC-AAV1 was significantly different YAC-AAV-CTL and AAV-HBKO at 3 mo. post injection; two-way ANOVA with repeated measures; $p < .05$). In contrast, AAV2-HBKO-miRNA-HTT treated mice showed no improvement in Rotarod performance across the study and there was no significant difference compared to YAC128 mice treated with the control vector AAV1-CTL at any time point (two-way ANOVA with repeated measures,

Table 1
Levels of GFP expression in mouse brain regions with AAV1 and AAV2-HBKO capsids.

Vector	CNS regions							
	Cortex	Striatum	Thalamus	Hippocampus	STN	SN	Medulla	Cerebellum
AAV1	+ + + +	+ + + + +	+ + + +	+ + +	+ + + +	+ + + +	+	+
AAV2-HBKO	+ + + +	+ + + + +	+ + + + +	+ + + +	+ + + +	+ + + +	+ +	+ +

AAV1 generated robust GFP expression in mouse cortical and subcortical regions including striatum, thalamus, hippocampus, as well as subthalamic nuclei and substantia nigra. Less GFP expression was detected in hindbrain regions such as medulla and cerebellum.

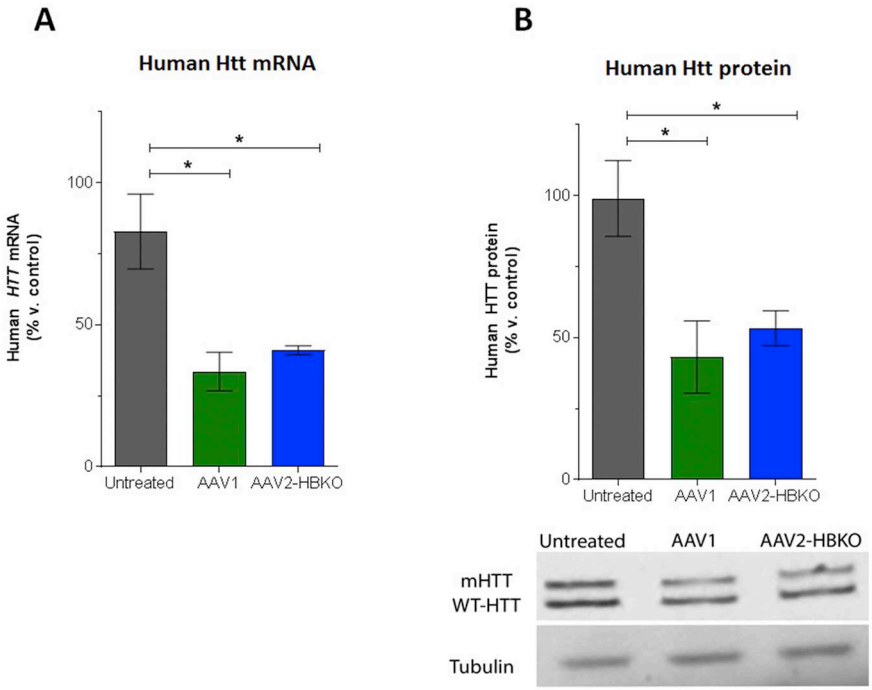

Fig. 2. AAV1- and AAV2-HBKO-eGFP-miRNA-Htt mediates the reduction of HTT levels in YAC128 mice. Adult YAC128 mice received bilateral intra-striatal injections of AAV1-eGFP-miRNA-HTT ($5 \times 10E^{12}$ VG/ml) ($N = 6$) or AAV2-HBKO-eGFP-miRNA-HTT ($2.2 \times 10E^{12}$ vg/ml) ($N = 6$), and brains were analyzed 1 month post-injection using both qPCR and western blot. (A) QPCR analysis revealed that levels of mutant human HTT mRNA in the striatum were significantly reduced in the AAV1 and AAV2-HBKO injected mice when compared to untreated controls. (B) Western blots demonstrate a commensurate reduction in human HTT protein levels in the striatum of YAC128 mice. Tubulin is shown as a loading control. Graphs represent a densitometric analysis of Western blots normalized to tubulin and are presented as percentage of untreated control. p-value < .05 was considered statistically significant. One-way ANOVA, Tukey's post-hoc; Untreated vs. AAV1: *$p < .05$P, Untreated vs. AAV2-HBKO: *$p < .05$.

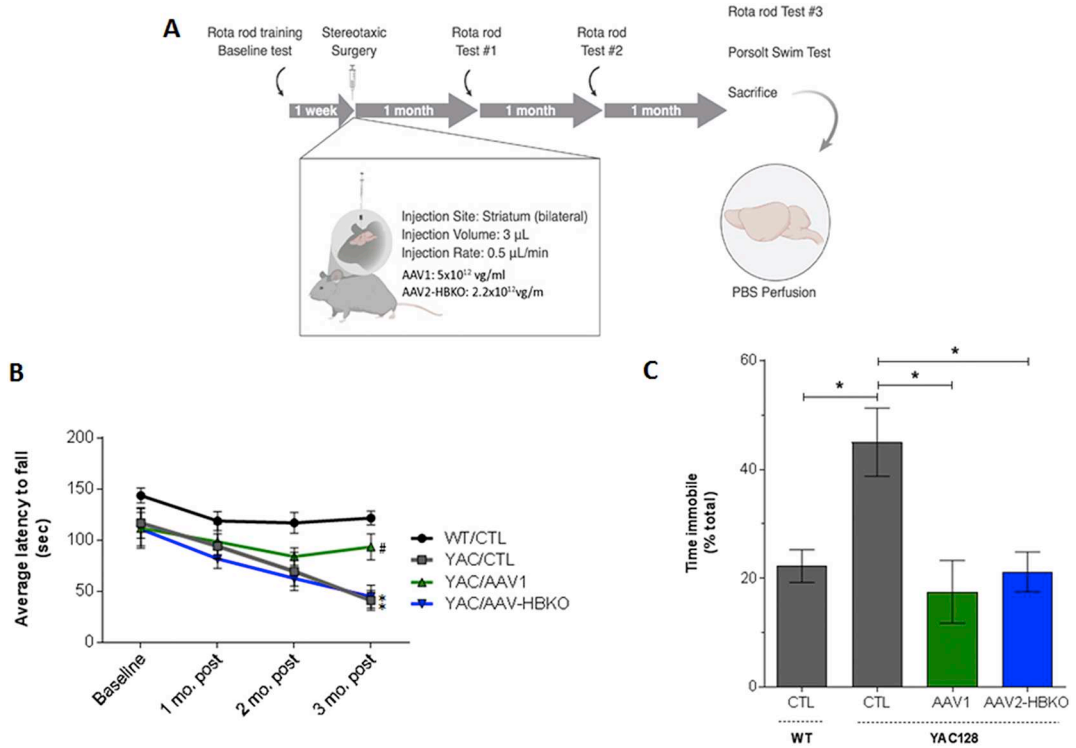

Fig. 3. The effects of striatal administration of AAV1-miRNA-Htt and AAV2-HBKO on behavioral deficits of YAC128 mice. (A) Illustration of the experimental timeline (generated with BioRender). Two-month-old YAC128 and wild-type (WT) mice received bilateral striatal injections of either AAV1-miRNA-Htt (4.5×10^{12} vg/ml) (YAC, $N = 12$), AAV2-HBKO-miRNA-HTT (4.0×10^{12} vg/ml) (YAC, $N = 12$) or AAV2/1-CTL control (3.0×10^{12} vg/ml) (YAC, $N = 11$; WT, $N = 12$) and were subjected to a Rotarod test and the Porsolt swim test at time points following surgery as indicated. All mice were sacrificed 3 months following surgery and tissues were then collected for biochemical analyses. (B) Accelerating Rotarod test 2 months after the injection of AAV1-miRNA-Htt. * Two-way ANOVA, significant effect of treatment and time point; $p < .05$, YAC-AAV-CTL and AAV-HBKO significantly different WT, $p < .05$; two-way ANOVA with repeated measures. Values are given as means ± SEM. (C) Time spent immobile in the PST 3 months after the injection of AAV1-miRNA-Htt. Values are given as means ± SEM. *Significant difference from control, $p < .05$; One-way ANOVA followed by Tukey post-hoc test.

p = NS) (Fig. 3B).

2.4. AAV1 and AAV2-HBKO improves the depressive phenotype in Porsolt Swim Test 3 months post injection

Previous reports indicate that YAC128 mice exhibit a depressive phenotype as early as 3 months of age that can be detected using the Porsolt Swim Test (PST) (Pouladi et al., 2009). Animals are deemed to exhibit a depressive state if they are immobile for an extended period of time when placed into a container of water. Using a basic swim speed test (where swim latency to reach a platform was measured) researchers have demonstrated that this depressive phenotype in the PST is unrelated to the swimming ability of YAC128 mice and is independent of the well documented motor coordination deficits observed in this model (Pouladi et al., 2009). YAC128 and WT littermate mice injected with AAV1-, AAV2-HBKO-miRNA-HTT, or AAV1-CTL-miRNA-HTT-vectors were tested 3 months post injection in the PST (Fig. 3A). Control treated YAC128 mice (YAC128-AAV1-CTL) displayed a depressive phenotype as demonstrated by an increased period of time in an immobile state when compared to wild type control treated mice (WT AAV1-CTL) (One-way ANOVA, $p < .05$) (Fig. 3C). YAC128 mice injected with AAV1- or AAV2-HBKO-miRNA-HTT spent significantly less time in an immobile state than AAV1-CTL-treated controls and performance of AAV1- and AAV2-HBKO-miRNA-HTT treated YAC128 mice was similar to that of their wild-type littermates, suggesting a near-complete correction of this aberrant phenotype (One-way ANOVA, $p < .05$) (Fig. 3C).

2.5. AAV1- and AAV2-HBKO-miRNA-HTT results in a significant decrease in human and mouse HTT mRNA and protein levels 3 months post injection

The striatal levels of mutant human HTT and endogenous mouse HTT mRNA and protein from mice that underwent behavioral testing were analyzed 3 months post injection. Both human HTT and mouse HTT mRNA were significantly reduced in the AAV1-miRNA-HTT and AAV2-HBKO-miRNA-HTT-injected mice when compared to AAV1-CTL-treated controls (One-way ANOVA, $*p < .01$) (Fig. 4A,B). Striatal human and mouse HTT protein levels were significantly reduced by western blot following injection of both AAV1 and AAV2-HBKO to AAV1-CTL-treated controls (One-way ANOVA, $*p < .01$) (Fig. 4B,E). Levels of human and mouse HTT protein were evaluated in the cortical region directly above the striatal injection site. Human mHTT protein levels were significantly reduced in the cortex following injection of both AAV1 and AAV2-HBKO compared to AAV1-CTL-treated controls (One-way ANOVA, $*p < .01$) (Fig. 4C). Mouse HTT protein levels were only significantly reduced in the cortex following injection of AAV2-HBKO (One-way ANOVA, $*p < .01$)(Fig. 4F). AAV1-miRNA-HTT showed a trend towards reduction of mouse HTT in the cortex but these

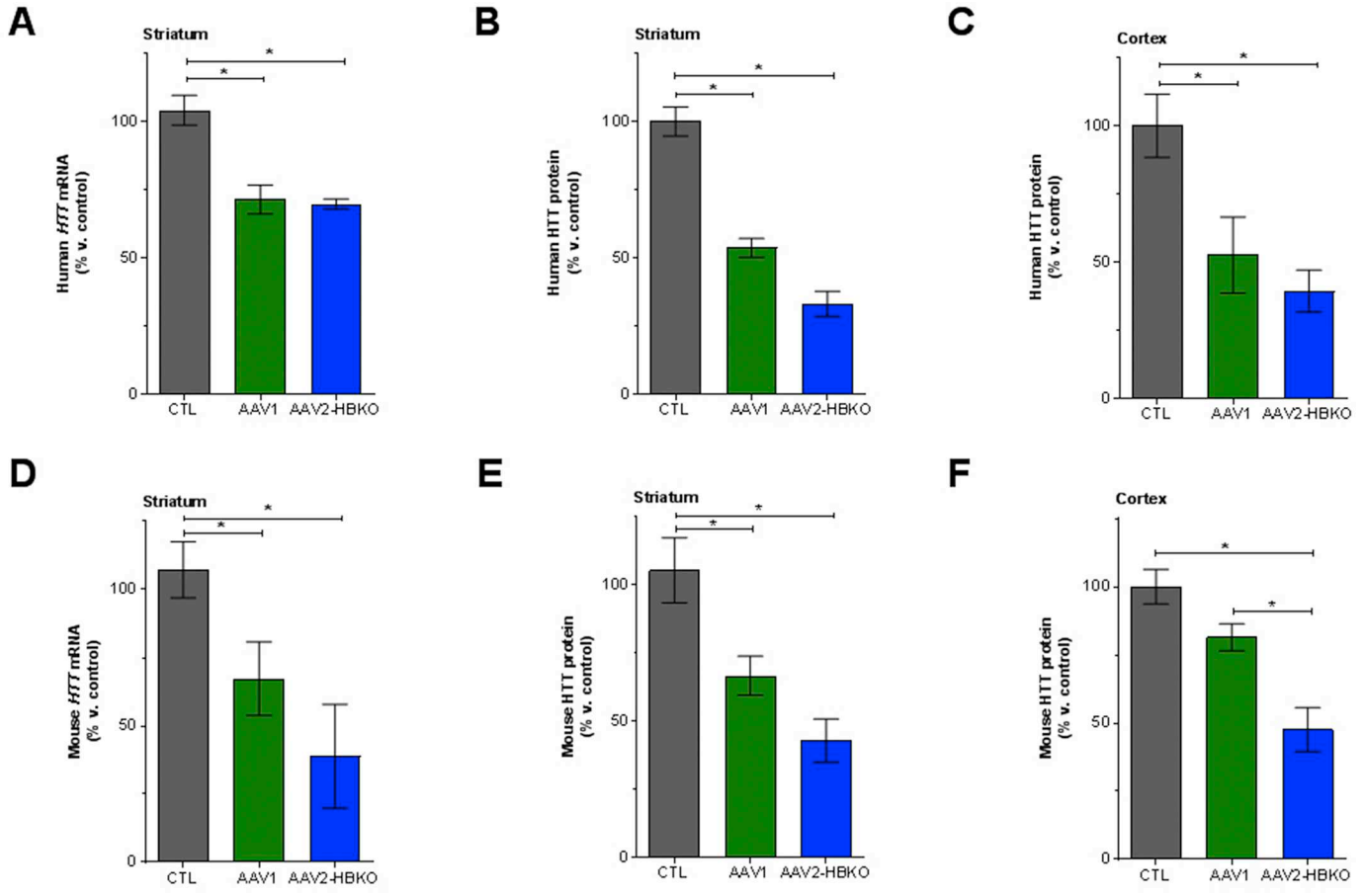

Fig. 4. AAV1-and AAV2-HBKO-miRNA-Htt mediates the reduction of HTT levels in YAC128 Mouse brain.
(A) Quantitative PCR analysis evaluating human mutant HTT mRNA levels in the striatum 3 months post injection of AAV1-and AAV2-HBKO-miRNA-Htt. HPRT served as a normalization control gene. (B) Human mutant HTT protein levels in the striatum as measured by Western blot 3 months after AAV injection. (C) Human mutant HTT protein levels in the cortex as measured by Western blot 3 months after AAV injection. (D) Quantitative PCR analysis evaluating mouse HTT mRNA levels in the striatum 3 months post injection of AAV1-and AAV2-HBKO-miRNA-Htt. HPRT served as a normalization control gene. (E) Mouse HTT protein levels in the striatum as measured by Western blot 3 months after AAV injection. (F) Mouse HTT protein levels in the cortex as measured by Western blot 3 months after AAV injection. All values are given as means ± SEM. * All values are given as means ± SEM. *Significant difference, $p < .05$; One-way ANOVA followed by Tukey post-hoc test.

levels did not reach statistical significance (Fig. 4F).

3. Discussion

The present study provides further evidence implicating an important role for astrocytes in the pathophysiology of Huntington's disease. Astrocytes are known to play key roles within neural circuits, but it remains unclear whether they contribute to, or perhaps even drive disease mechanisms in HD. There is a wealth of evidence suggesting the presence of mHTT in astrocytes leads to decreased expression of glutamate transporters and altered glutamate uptake which is sufficient to induce neurodegeneration in medium spiny neurons of the striatum (Bradford et al., 2009; Bradford et al., 2010). Altered neuronal excitability and excitotoxicity associated with HD may therefore be a consequence of changes in astrocyte function (Tong et al., 2014; Skotte et al., 2018). Astrogliosis is widely accepted as a late-stage driver of neurodegeneration in HD, however astrocytes have not been viewed as participants in the early events leading to neuronal pathology. Animal models have been developed to evaluate the contribution of mHTT expression in astrocytes by driving the expression of the mutant protein with the human *GFAP* promoter (Hebb et al., 1999; Wang et al., 2008; Bradford et al., 2009; Meunier et al., 2016) These studies demonstrate that expression of mHTT in astrocytes may drive neurological phenotypes and exacerbate the effect of mHTT expression in neuronal cells and highlight a potential key role of glial cells in HD pathophysiological mechanisms (Chan and Surmeier, 2014; Khakh and Sofroniew, 2014).

Here we provide further evidence that HD involves a complex interplay between astrocytes and neurons, and mHTT mediated astrocyte dysfunction need to be considered in the development of HTT lowering therapeutic strategies. In order to gain a better understanding of the contribution of astrocytes to HD pathophysiology, distinct AAV capsids were employed to deliver a therapeutic miRNA to specific cells types in order to assess the contribution of HTT lowering in neurons vs neurons and astrocytes on HD phenotypes. Previously it was demonstrated that AAV-RNAi mediated HTT reduction using the AAV1 capsid (which transduces both neurons and astrocytes) is capable of ameliorating HD phenotypes in the YAC128 mouse model of HD (Stanek et al., 2014). Here we corroborate those findings using the AAV1 vector and extend these findings to show that AAV-mediated HTT reduction in neurons alone was not sufficient to support complete therapeutic benefit in the YAC128 mouse. Both AAV1 and AAV2-HBKO vectors confer widespread transduction throughout the injected striatum as well as adjacent cortical regions. Double labeling studies with neuronal and astrocytic markers confirmed that AAV2-HBKO exclusively transduced neuronal cells with minimal (if any) transduction of astrocytes, while AAV1 transduced both neurons and astrocytes. YAC128 mice show a progressive Rotarod deficit that was not ameliorated when mHTT levels were reduced only in neurons, as evidenced by the lack of Rotarod improvement in mice injected with AAV2-HBKO-miRNA-HTT vector (a vector with comparable distribution as AAV1 but exclusively neuronal tropism). Consistent to previous findings, mice that received AAV1 did not develop a progressive impairment in Rotarod performance and at 6 months of age were not statistically different from WT mice.

In the YAC128 mouse model, neural dysfunction and striatal cell loss is highly correlated with Rotarod performance, thus there is a clear structural correlate for this behavioral phenotype (Van Raamsdonk et al., 2005; Van Raamsdonk et al., 2007; Martin et al., 2013; Burnham et al., 2015). If MSN's excitotoxicity is caused in part by mHTT toxicity in astrocytes, suggesting that ameliorating mHTT toxicity in astrocytes would ameliorate MSN dysfunction, preserve striatal cells, and impact the Rotarod deficit in the YAC128 model was observed. Interestingly, the same phenomenon was not observed for the well characterized depressive phenotype in YAC128 mice as measured by the Porsolt Swim Test (PST) (Porsolt et al., 1977). The PST is a widely used rodent behavioral assay, in which the immobility of animals is used to assess the effectiveness of antidepressant drugs (Dufour et al., 2014; Khakh and Sofroniew, 2014). Depression and related mood disturbances are prevalent not only among HD patients but also in pre-symptomatic carriers of the mutant allele. To date the pathophysiology underlying these psychiatric symptoms are poorly understood (Julien et al., 2007; Chan and Surmeier, 2014; Chiocco et al., 2014). YAC128 mice treated with the control vector show significantly higher levels of immobility (also known as behavioral despair) compared to WT mice. AAV1 and AAV2-HBKO animals both showed immobility levels comparable to WT mice suggesting that HTT reduction in neurons alone was sufficient to rescue this behavioral deficit. The anatomical basis of this behavioral phenotype is not clearly defined but likely involves the prefrontal cortex and dorsal raphe nucleus, among other regions, which are all transduced with both AAV1 and AAV2-HBKO vectors. Our study suggests the depressive phenotype in the YAC128 mouse model is driven largely by neuronal dysfunction and highlights that possibility that mHTT mediated dysfunction in different cell types may underlie distinct features of HD phenotypes. While we demonstrate that mHTT levels are reduced by approximately 50% in the striatum of animals injected with either AAV1 or AAV2-HBKO we don't yet know the extent of HTT reduction in any given cell type and differential HTT reduction in neurons versus astrocytes by AAV-RNAi warrants further investigation. Cell sorting in conjunction with single cell sequencing may provide interesting insights to the extent of HTT lowering required in distinct cell types for prevention of HD pathogenesis.

The idea that distinct cell types may be preferentially involved in different aspects of HD pathology is further highlighted by a study performed using systemic administration of an AAV9 HTT-lowering vector in the N171-82Q HD mouse model. Intrajugular delivery of AAV9-miRNA-HTT resulted in significant reduction in HTT levels throughout the brain however there was preferential transduction of neurons in some brain regions (hippocampus, hypothalamus, and cerebellum), while in subcortical regions (thalamus, striatum, globus pallidus) there was preferential transduction of astrocytes (Dufour et al., 2014). Despite the significant HTT reduction in the brain there was no rescue of the Rotarod deficit in these mice, consistent with our findings that both neurons and astrocytes need to be transduced to ameliorate this behavioral deficit. Interestingly other disease phenotypes such as brain atrophy were significantly improved in this study further indicating the complex interplay of neurons and astrocytes that may be an underappreciated component of HD disease biology (Dufour et al., 2014).

Another cell type which has been implicated to play a role in HD pathology is the oligodendrocyte. A link has been demonstrated between myelin breakdown and the onset of HD using both postmortem human tissue and in vivo imaging. It is believed that premature myelin breakdown and subsequent homeostatic remyelination attempts may contribute to HD pathogenesis and neuronal loss (Bartzokis et al., 2007). Mutant huntingtin is present in oligodendrocytes and HD mice transgenic mice that selectively express mutant huntingtin in oligodendrocytes show progressive neurological symptoms and early death, as well as age-dependent demyelination and reduced expression of myelin genes that are downstream of myelin regulatory factor (Huang et al., 2015). While there is still more to learn on the role of oligodendrocytes in HD they may also make an important therapeutic target and should be further investigated. Unfortunately there are no naturally occurring AAV serotypes which can efficiently transduce large numbers of Oligodendrocytes in the CNS. With advances in AAV capsid engineering and the evolution of novel capsids with selective tropism this may soon be possible.

To date, research efforts have been focused largely on identifying neuronal mechanisms to account for HD related changes in HD models. Our findings provide evidence that astrocytes play a key role in some aspects of HD pathogenesis and must be contemplated in the design of HD therapeutics. It would be ideal to evaluate AAV vectors with a strong preferential tropism to astrocytes and compare selective HTT reduction in astrocytes to results to those obtained here. Unfortunately

such a naturally occurring AAV vector does not exist to our knowledge. GFAP promoters can be used to drive expression of AAV in astrocytes however the promoter will also affect the strength of AAV transduction to a level that would not be comparable to the AAV1 and AAV2 HBKO vectors used here with the very strong CBA promoter. Novel AAV capsids are currently being identified which demonstrate selective tropism for astrocytes and can be used in conjunction with the CBA promoters. These novel capsids are still under development and once available it would be interesting to make direct comparisons to the data reported here.

Therapeutics that target only neurons may be inadequate at restoring normal function and ameliorating all disease pathophysiology. Considering the high flexibility of viral vector approaches, the present study not only provides interesting insights about the contribution of astrocytes to the pathophysiology of HD, but also reveals the necessity to consider the cell type specificity for HTT lowering therapeutics. Future studies employing single cell RNA sequencing of neurons and astrocytes are warranted. Not only would studies of this nature help delineate the extent of HTT reduction in each cell type but it may also provide insight about specific dysfunction in astrocytes versus neurons that may contribute to disease pathology.

4. Methods

4.1. Generation of variant AAV2 capsid plasmid

Mutagenesis was performed using the QuikChange Lightning Multi Site-Directed Mutagenesis kit (Agilent Technologies, Santa Clara, CA), according to the manufacturer's protocol. The pIM45BD plasmid was used to generate AAV2-HBKO using a PCR mutagenesis primer designed to alter the codons encoding arginine 585 and 588 on VP3 to alanine. The sequence of the mutagenic primer used to generate the R585A and R588A mutations was as follows: TATCTACCAACCTCCAGGCAGGCAA CGCACAAGCAGCTACCGCAG. Mutations were confirmed by DNA sequencing.

4.2. Production of AAV-eGFP vectors

Recombinant AAV vectors encoding eGFP under the control of the CBA promoter were produced using the transient transfection method, as previously described (Xiao et al., 1998). Briefly, HEK293 cells were transfected using polyethyleneimine (PEI) with a 1:1:1 ratio of the three plasmids (containing the ITR, AAV rep/cap and Ad helper). The Ad helper plasmid (pHelper) was obtained from Stratagene/Agilent Technologies (Santa Clara, CA). Purification was performed using column chromatography, as previously described (Martin et al., 2013; Burnham et al., 2015). The resulting titer of AAV1-eGFP was determined to be 5.0×10^{12} vg/ml and the titer of AAV2-HBKO-eGFP was 2.2×10^{12} vg/ml using quantitative PCR (vector titer differences are within the error of the PCR vector titer assay).

4.3. miRNA plasmids and viral vectors

To generate recombinant AAV serotype vectors encoding a miRNA-based hairpin against the huntingtin gene (AAV-miRNA-HTT), the cDNA for human *HTT* was cloned into a shuttle plasmid containing the AAV inverted terminal repeats (ITR) and the 1.6-kb cytomegalovirus enhancer/chicken β-actin (CBA) promoter. Control vectors contained a noncoding miRNA sequence (designed to little to no possible matches across the transcriptome) (AAV1-CTL) or expressed an enhanced green fluorescent protein under the control of the same promoter (AAV1-eGFP-miRNA-HTT and AAV2-HBKO-eGFP-miRNA-HTT). All viral vectors were generated by the triple-plasmid co-transfection of human 293 cells, and the recombinant virions were column purified as previously described (Passini and Wolfe, 2001). The resulting titers of miRNA containing vectors were as follows: AAV1-miRNA-HTT = 4.5×10^{12} vg/ml, AAV1-CTL = 3.0×10^{12} vg/ml, and AAV2-HBKO-miRNA-HTT = 4×10^{12} vg/ml using quantitative PCR. AAV1-eGFP-miRNA-HTT and AAV2-HBKO-eGFP-miRNA-HTT titers were 5×10^{12} vg/ml and 2.2×10^{12} vg/ml respectively. Vectors titer values were all within the range of error of the PCR vector titer assay.

4.4. Animals

All procedures were performed using a protocol approved by the Institutional Animal Care and Use Committee at Sanofi (Department of Health and Human Services, NIH Publication 86–23). Mice used included YAC128 mice (a yeast artificial chromosome harboring the full-length human mutant *HTT* transgene with 128 CAG repeats on a pure FVB/NJ background) and wild type FVB/NJ littermate mice (Slow et al., 2003; Van Raamsdonk et al., 2005). Both the YAC128 mice and FVB/NJ littermates were obtained from a Sanofi colony that was housed at the Charles River Laboratories. The mice were maintained on a 12 h light/dark cycle with food and water available ad libitum. All behavioral testing was performed during the animals' light cycle (between the hours of 8 am and 4 pm). *N*-values for all experiments are included in the results section.

4.5. Surgical procedures

Animals were anesthetized using 3% isofluorane and placed into a stereotaxic frame. Intracranial injections were performed as previously described (Stanek et al., 2014). Three microliters of recombinant viral vectors were injected into the striatum (AP, +0.50; ML, ± 2.2; DV, −3.0 from bregma and dura; incisor bar, 0.0) using a 10 µl Hamilton syringe at the rate of 0.5 µl/min. The needle was left in place for 1 min following the completion of infusion. One hour before surgery and for 24 h following surgery, the mice were administered sustained release Buprenorphine SR-LAB (1.0 mg/kg) subcutaneously for analgesia.

4.6. Behavioral analysis

Rota Rod: Motor coordination and motor learning were assessed on an accelerating rotating rod apparatus (UgoBasile). At baseline mice were trained with 3 trials per day for 3 consecutive days with the Rota Rod accelerating from 5 to 40 rpm over 5 min with a maximum score of 300 s. On the third day (Test) data was collected over 3 trials and the latency to fall was recorded. On subsequent time points mice were tested for one day with the same parameters as Day 3 baseline.

Porsolt Swim Test: Mice were placed in a glass cylinder (20 cm height × 10 cm diameter) filled with water at 23 °C, up to a height of 7.5 cm. Total test time was 7 min. The test begins with a 3 min acclimation period followed by a 4 min observation period during which a blind observer records time spent swimming and time spent immobile. A mouse was judged to be immobile when it was floating almost motionless in the water.

4.7. Animal perfusion and tissue collection

Mice were perfused through the heart with phosphate-buffered saline (PBS) to remove all blood. For eGFP distribution experiments the brains were cut along the sagittal plane, post-fixed in 4% paraformaldehyde and 40-µm sections were cut using a vibratome. For miRNA efficacy studies brains were cut sagittally along the midline and the left hemisphere was post-fixed in 4% paraformaldehyde followed by 30% sucrose and then sectioned into 20-µm sections using a cryostat. The right hemisphere (used for biochemical assays) was cut along the coronal axis using a mouse brain matrix (Harvard Apparatus, Holliston, MA) and striatal and cortical regions were dissected using a 3 mm biopsy punch. Brain tissue was then flash-frozen in liquid nitrogen and stored at −80 °C until use.

4.8. Quantitative real-time PCR (TaqMan)

RNA levels were measured by quantitative real-time RT-PCR. Striatal punches were used for all RT-PCR analysis. Total RNA was extracted using the QIAGEN RNeasy mini kit and then reverse transcribed and amplified using the TaqMan® One-Step RT-PCR Master Mix Kit (Applied Biosystems) according to the manufacturer's instructions. Quantitative RT-PCR reactions were conducted and analyzed on an ABI PRISM® 7500 Real Time PCR System (Applied Biosystems). The expression levels of HTT mRNA were normalized to hypoxanthine guanine phosphoribosyl transferase 1 (Hprt1) mRNA levels. Standard curves were generated using 5-fold serial dilutions of mouse brain cDNA. Each sample was run in duplicate. The relative gene expression was determined by using the $\Delta\Delta C_T$ method and normalizing to Hprt1 mRNA levels. Efficiency measured as 92.45% based on −3.5172 slope. Mouse HTT primer: Mm01213820_M1 Htt FAM (Applied Biosystems). Mouse Hprt primer: Mm00446968_M1 Hprt FAM (Applied Biosystems). Custom made Human HTT primer: Reverse: GGAAATCAGAACCCTCA AATGG; Forward: CTCCGTCCGGTAGACATGT (Applied Biosystems).

4.9. Western blotting

Protein levels were measured by western blot analysis. Striatal and cortical tissue punches were used for all western blot analysis. Tissues, at a final concentration of 50 mg/ml in T-Per lysis buffer (Thermofisher) and containing the complete protease inhibitor cocktail (Roche), were homogenized. The homogenates were cleared by centrifugation at 10,000 ×*g* for 6 min at 4 °C. The protein concentration was measured by using BSA assay (Pierce). Twenty to thirty micrograms of the homogenates was resolved on a 3–8% Novex tris-acetate gel and then transferred to a nitrocellulose membrane. The membranes were probed with a mouse anti-huntingtin monoclonal antibody (Mab2166 Millipore; 1:2000 dilution,) and rabbit polyclonal anti-β-tubulin antibody (1:750 dilution, Santa Cruz Biotechnology). The membranes were then incubated with infrared secondary antibodies (1:20,000 dilution, Rockland), and the proteins were visualized by quantitative fluorescence using an Odyssey imager (LI-COR Biosciences). To control for loading variances, HTT protein was normalized to β-tubulin and expressed as a percentage of control animals. Molecular weight markers were used to verify the identity of the proteins.

4.10. Immunohistochemistry

Vibratome brain sections were stained with the mouse anti-NeuN monoclonal antibody (catalog #MAB377; Millipore) diluted 1:500 in Da Vinci Green Diluent (catalog #PD900; Biocare Medical) to identify neuronal nuclei. An Alexa Fluor 555-conjugated donkey anti-mouse antibody (catalog #A31570; ThermoFisher) diluted 1:200 in fluorescent antibody diluent (catalog #FAD901; Biocare Medical) was used as a secondary antibody. Sections were incubated with 0.1% Sudan Black B (catalog #199664; Sigma-Aldrich) to reduce autofluorescence. For astrocyte, microglia or oligodendrocyte stainings, sections were incubated with a rabbit anti-GFAP antibody (catalog #Z033429–2, Agilent, 1:1000 dilution), rabbit anti-IBA1 antibody (catalog #019–19,741, Wako, 1:500 dilution) or goat anti-Olig2 (catalog#AF2418, R&D Systems, 1:500 dilution), respectively, followed by incubation in Alexa Fluor 555 conjugated anti-rabbit or anti-goat secondary antibody (catalog #A31572 or #A21423, ThermoFisher, 1:200 dilution). For GFP immunostaining, vibratome brain sections were incubated with a rabbit anti-eGFP antibody (Millipore; 1:500 dilution), followed by a biotinylated anti-rabbit secondary antibody (Jackson Laboratories; 1:250 dilution), and the immunopositive signal was visualized using a diaminobenzidine detection method according to the manufacturer's protocol (Vector Lab, Vectorstain ABC-HRP Kit, PK4001). All sections were analyzed using a Leica DM5500 confocal microscope.

4.11. Cell quantification

The percent neuronal and glial transduction was estimated in the brain striatum and frontal cortex regions. The numbers of GFP positive cells that also express GFAP or NeuN were counted on two separate sections at least 200 um apart per animal, and at least 200–300 GFP positive cells were assessed per section. The numbers represent average cell counts from 4 mice.

4.12. Statistics

Mean values were used for statistical analyses. Data are expressed as the mean ± SEM. Statistical analysis was performed using Prism version 5.0 (GraphPad Software, Inc.). Data were analyzed using Student's *t*-test and one- or two-way analysis of variance (ANOVA), followed by post-hoc Tukey multiple comparison when appropriate. For comparison of two $p < .05$ was considered a statistically significant difference.

Author contributions

LS: Experimental design, performed studies, data analysis, wrote manuscript.

JB: Performed studies, generated figures, reviewed and edited manuscript.

LS: Experimental design, data review, manuscript preparation and editing.

Acknowledgements

The authors thank C. O'Riordan, J. Sullivan, D. Woodcock, S. Nass, and M. Mattingly for AAV vector generation and production and T. Taksir, R. Karolides, L. Curtin, S. Savage, B. Mastis, and J. E. Irazoqui for technical assistance and support.

References

Acuña, A.I., Esparza, M., Kramm, C., Beltrán, F.A., Parra, A.V., Cepeda, C., Toro, C.A., Vidal, R.L., Hetz, C., Concha, I.I., Brauchi, S., Levine, M.S., Castro, M.A., 2013. A failure in energy metabolism and antioxidant uptake precede symptoms of Huntington's disease in mice. Nat. Commun. 4, 2917.

Arnett, A.L., Beutler, L.R., Quintana, A., Allen, J., Finn, E., Palmiter, R.D., Chamberlain, J.S., 2013. Heparin-binding correlates with increased efficiency of AAV1- and AAV6-mediated transduction of striated muscle, but negatively impacts CNS transduction. Gene Ther. 20, 497–503.

Aronin, N., DiFiglia, M., 2014. Huntingtin-lowering strategies in Huntington's disease: antisense oligonucleotides, small RNAs, and gene editing. Mov. Disord.: Off. J. Mov. Disord. Soc. 29, 1455–1461.

Bartzokis, G., Lu, P.H., Tishler, T.A., Fong, S.M., Oluwadara, B., Finn, J.P., Huang, D., Bordelon, Y., Mintz, J., Perlman, S., 2007. Myelin breakdown and iron changes in Huntington's disease: pathogenesis and treatment implications. Neurochem. Res. 32, 1655–1664.

Belanger, M., Allaman, I., Magistretti, P.J., 2011. Brain energy metabolism: focus on astrocyte-neuron metabolic cooperation. Cell Metab. 14, 724–738.

Benraiss, A., Wang, S., Herrlinger, S., Li, X., Chandler-Militello, D., Mauceri, J., Burm, H.B., Toner, M., Osipovitch, M., Jim Xu, Q., Ding, F., Wang, F., Kang, N., Kang, J., Curtin, P.C., Brunner, D., Windrem, M.S., Munoz-Sanjuan, I., Nedergaard, M., Goldman, S.A., 2016. Human glia can both induce and rescue aspects of disease phenotype in Huntington disease. Nat. Commun. 7, 11758.

Boudreau, R.L., McBride, J.L., Martins, I., Shen, S., Xing, Y., Carter, B.J., Davidson, B.L., 2009. Nonallele-specific silencing of mutant and wild-type huntingtin demonstrates therapeutic efficacy in Huntington's disease mice. Mol. Ther.: J. Am. Soc. Gene Ther. 17, 1053–1063.

Bradford, J., Shin, J.Y., Roberts, M., Wang, C.E., Li, X.J., Li, S., 2009. Expression of mutant huntingtin in mouse brain astrocytes causes age-dependent neurological symptoms. Proc. Natl. Acad. Sci. U. S. A. 106, 22480–22485.

Bradford, J., Shin, J.Y., Roberts, M., Wang, C.E., Sheng, G., Li, S., Li, X.J., 2010. Mutant huntingtin in glial cells exacerbates neurological symptoms of Huntington disease mice. J. Biol. Chem. 285, 10653–10661.

Burnham, B., Nass, S., Kong, E., Mattingly, M., Woodcock, D., Song, A., Wadsworth, S., Cheng, S.H., Scaria, A., O'Riordan, C.R., 2015. Analytical ultracentrifugation as an approach to characterize recombinant adeno-associated viral vectors. Hum. Gene Ther. Methods 26, 228–242.

Chan, C.S., Surmeier, D.J., 2014. Astrocytes go awry in Huntington's disease. Nat. Neurosci. 17, 641–642.

Chiocco, M., Choi, V., Graham, A., Klatte, D., Francone, O., Thomson, D., Zeitler, B.,

Froelich, S., Yu, Q., E Paschon, D., C Miller, J., Marlen, K., J Rebar, E., D Urnov, F., Gregory, P., Zhang, H., 2014. A7 drug discovery approach for rare neurological diseases: using novel zinc finger protein technology to develop potential therapy for Huntington's disease. J. Neurol. Neurosurg. Psychiatry 85 (12), 1411–1418.
Cudkowicz, M., Kowall, N.W., 1990. Degeneration of pyramidal projection neurons in Huntington's disease cortex. Ann. Neurol. 27, 200–204.
Dufour, B.D., Smith, C.A., Clark, R.L., Walker, T.R., McBride, J.L., 2014. Intrajugular vein delivery of AAV9-RNAi prevents neuropathological changes and weight loss in Huntington's disease mice. Mol. Ther.: J. Am. Soc. Gene Ther. 22, 797–810.
Gray, S.J., Woodard, K.T., Samulski, R.J., 2010. Viral vectors and delivery strategies for CNS gene therapy. Ther. Deliv. 1, 517–534.
Hadaczek, P., Stanek, L., Ciesielska, A., Sudhakar, V., Samaranch, L., Pivirotto, P., Bringas, J., O'Riordan, C., Mastis, B., San Sebastian, W., Forsayeth, J., Cheng, S.H., Bankiewicz, K.S., Shihabuddin, L.S., 2016. Widespread AAV1- and AAV2-mediated transgene expression in the nonhuman primate brain: implications for Huntington's disease. Mol. Ther. Methods Clin. Dev. 3, 16037.
Hebb, M.O., Denovan-Wright, E.M., Robertson, H.A., 1999. Expression of the Huntington's disease gene is regulated in astrocytes in the arcuate nucleus of the hypothalamus of postpartum rats. FASEB J.: Off. Publ. Fed. Am. Soc. Exp. Biol. 13, 1099–1106.
Huang, B., Wei, W., Wang, G., Gaertig, M.A., Feng, Y., Wang, W., Li, X.J., Li, S., 2015. Mutant huntingtin downregulates myelin regulatory factor-mediated myelin gene expression and affects mature oligodendrocytes. Neuron 85, 1212–1226.
Jiang, R., Diaz-Castro, B., Looger, L.L., Khakh, B.S., 2016. Dysfunctional calcium and glutamate signaling in striatal astrocytes from Huntington's disease model mice. J. Neurosci. 36, 3453–3470.
Julien, C.L., Thompson, J.C., Wild, S., Yardumian, P., Snowden, J.S., Turner, G., Craufurd, D., 2007. Psychiatric disorders in preclinical Huntington's disease. J. Neurol. Neurosurg. Psychiatry 78, 939–943.
Keiser, M.S., Kordasiewicz, H.B., McBride, J.L., 2016. Gene suppression strategies for dominantly inherited neurodegenerative diseases: lessons from Huntington's disease and spinocerebellar ataxia. Hum. Mol. Genet. 25, R53–R64.
Khakh, B.S., Sofroniew, M.V., 2014. Astrocytes and Huntington's disease. ACS Chem. Neurosci. 5, 494–496.
Khakh, B.S., Beaumont, V., Cachope, R., Munoz-Sanjuan, I., Goldman, S.A., Grantyn, R., 2017. Unravelling and exploiting astrocyte dysfunction in Huntington's disease. Trends Neurosci. 40, 422–437.
Kordasiewicz, H.B., Stanek, L.M., Wancewicz, E.V., Mazur, C., McAlonis, M.M., Pytel, K.A., Artates, J.W., Weiss, A., Cheng, S.H., Shihabuddin, L.S., Hung, G., Bennett, C.F., Cleveland, D.W., 2012. Sustained therapeutic reversal of Huntington's disease by transient repression of huntingtin synthesis. Neuron 74, 1031–1044.
Lobsiger, C.S., Cleveland, D.W., 2007. Glial cells as intrinsic components of non-cell-autonomous neurodegenerative disease. Nat. Neurosci. 10, 1355–1360.
Malankhanova, T.B., Malakhova, A.A., Medvedev, S.P., Zakian, S.M., 2017. Modern genome editing technologies in Huntington's disease research. J. Huntingt. Dis. 6, 19–31.
Maragakis, N.J., Rothstein, J.D., 2001. Glutamate transporters in neurologic disease. Arch. Neurol. 58, 365–370.
Martin, J., Frederick, A., Luo, Y., Jackson, R., Joubert, M., Sol, B., Poulin, F., Pastor, E., Armentano, D., Wadsworth, S., Vincent, K., 2013. Generation and characterization of adeno-associated virus producer cell lines for research and preclinical vector production. Human Gene Ther. Methods 24, 253–269.
McBride, J.L., Pitzer, M.R., Boudreau, R.L., Dufour, B., Hobbs, T., Ojeda, S.R., Davidson, B.L., 2011. Preclinical safety of RNAi-mediated HTT suppression in the rhesus macaque as a potential therapy for Huntington's disease. Molecular therapy : the journal of the. Am. Soc. Gene Ther. 19, 2152–2162.
Merienne, N., Vachey, G., de Longprez, L., Meunier, C., Zimmer, V., Perriard, G., Canales, M., Mathias, A., Herrgott, L., Beltraminelli, T., Maulet, A., Dequesne, T., Pythoud, C., Rey, M., Pellerin, L., Brouillet, E., Perrier, A.L., du Pasquier, R., Deglon, N., 2017. The self-inactivating KamiCas9 system for the editing of CNS disease genes. Cell Rep. 20, 2980–2991.
Meunier, C., Merienne, N., Jolle, C., Deglon, N., Pellerin, L., 2016. Astrocytes are key but indirect contributors to the development of the symptomatology and pathophysiology of Huntington's disease. Glia 64, 1841–1856.
Miniarikova, J., Zimmer, V., Martier, R., Brouwers, C.C., Pythoud, C., Richetin, K., Rey, M., Lubelski, J., Evers, M.M., van Deventer, S.J., Petry, H., Deglon, N., Konstantinova, P., 2017. AAV5-miHTT gene therapy demonstrates suppression of mutant huntingtin aggregation and neuronal dysfunction in a rat model of Huntington's disease. Gene Ther. 24, 630–639.
Monteys, A.M., Spengler, R.M., Dufour, B.D., Wilson, M.S., Oakley, C.K., Sowada, M.J., McBride, J.L., Davidson, B.L., 2014. Single nucleotide seed modification restores in vivo tolerability of a toxic artificial miRNA sequence in the mouse brain. Nucleic Acids Res. 42, 13315–13327.
Naidoo, J., Stanek, L.M., Ohno, K., Trewman, S., Samaranch, L., Hadaczek, P., O'Riordan, C., Sullivan, J., San Sebastian, W., Bringas, J.R., Snieckus, C., Mahmoodi, A., Mahmoodi, A., Forsayeth, J., Bankiewicz, K.S., Shihabuddin, L.S., 2018. Extensive transduction and enhanced spread of a modified AAV2 capsid in the non-human primate CNS. Mol. Ther.: J. Am. Soc. Gene Ther. 26, 2418–2430.
Nana, A.L., Kim, E.H., Thu, D.C., Oorschot, D.E., Tippett, L.J., Hogg, V.M., Synek, B.J., Roxburgh, R., Waldvogel, H.J., Faull, R.L., 2014. Widespread heterogeneous neuronal loss across the cerebral cortex in Huntington's disease. J. Huntingt. Dis. 3, 45–64.
Passini, M.A., Wolfe, J.H., 2001. Widespread gene delivery and structure-specific patterns of expression in the brain after intraventricular injections of neonatal mice with an adeno-associated virus vector. J. Virol. 75, 12382–12392.
Porsolt, R.D., Le Pichon, M., Jalfre, M., 1977. Depression: a new animal model sensitive to antidepressant treatments. Nature 266, 730–732.
Pouladi, M.A., Graham, R.K., Karasinska, J.M., Xie, Y., Santos, R.D., Petersen, A., Hayden, M.R., 2009. Prevention of depressive behaviour in the YAC128 mouse model of Huntington disease by mutation at residue 586 of huntingtin. Brain: J. Neurol. 132, 919–932.
Ross, C.A., 2002. Polyglutamine pathogenesis: emergence of unifying mechanisms for Huntington's disease and related disorders. Neuron 35, 819–822.
Ross, C.A., Tabrizi, S.J., 2011. Huntington's disease: from molecular pathogenesis to clinical treatment. Lancet Neurol. 10, 83–98.
Shin, J.Y., Fang, Z.H., Yu, Z.X., Wang, C.E., Li, S.H., Li, X.J., 2005. Expression of mutant huntingtin in glial cells contributes to neuronal excitotoxicity. J. Cell Biol. 171, 1001–1012.
Skotte, N.H., Andersen, J.V., Santos, A., Aldana, B.I., Willert, C.W., Nørremølle, A., Waagepetersen, H.S., Nielsen, M.L., 2018. Integrative characterization of the R6/2 mouse model of Huntington's disease reveals dysfunctional astrocyte metabolism. Cell Rep. 23, 2211–2224.
Slow, E.J., van Raamsdonk, J., Rogers, D., Coleman, S.H., Graham, R.K., Deng, Y., Oh, R., Bissada, N., Hossain, S.M., Yang, Y.Z., Li, X.J., Simpson, E.M., Gutekunst, C.A., Leavitt, B.R., Hayden, M.R., 2003. Selective striatal neuronal loss in a YAC128 mouse model of Huntington disease. Hum. Mol. Genet. 12, 1555–1567.
Stanek, L.M., Yang, W., Angus, S., Sardi, P.S., Hayden, M.R., Hung, G.H., Bennett, C.F., Cheng, S.H., Shihabuddin, L.S., 2013. Antisense oligonucleotide-mediated correction of transcriptional dysregulation is correlated with behavioral benefits in the YAC128 mouse model of Huntington's disease. J. Huntingt. Dis. 2, 217–228.
Stanek, L.M., Sardi, S.P., Mastis, B., Richards, A.R., Treleaven, C.M., Taksir, T., Misra, K., Cheng, S.H., Shihabuddin, L.S., 2014. Silencing mutant huntingtin by adeno-associated virus-mediated RNA interference ameliorates disease manifestations in the YAC128 mouse model of Huntington's disease. Hum. Gene Ther. 25, 461–474.
Sullivan, J.A., Stanek, L.M., Lukason, M.J., Bu, J., Osmond, S.R., Barry, E.A., O'Riordan, C.R., Shihabuddin, L.S., Cheng, S.H., Scaria, A., 2018. Rationally designed AAV2 and AAVrh8R capsids provide improved transduction in the retina and brain. Gene Ther. 25, 205–219.
Tabrizi, S.J., Scahill, R.I., Durr, A., Roos, R.A., Leavitt, B.R., Jones, R., Landwehrmeyer, G.B., Fox, N.C., Johnson, H., Hicks, S.L., Kennard, C., Craufurd, D., Frost, C., Langbehn, D.R., Reilmann, R., Stout, J.C., Investigators, T.-H., 2011. Biological and clinical changes in premanifest and early stage Huntington's disease in the TRACK-HD study: the 12-month longitudinal analysis. Lancet Neurol. 10, 31–42.
Tong, X., Ao, Y., Faas, G.C., Nwaobi, S.E., Xu, J., Haustein, M.D., Anderson, M.A., Mody, I., Olsen, M.L., Sofroniew, M.V., Khakh, B.S., 2014. Astrocyte Kir4.1 ion channel deficits contribute to neuronal dysfunction in Huntington's disease model mice. Nat. Neurosci. 17, 694–703.
Van Raamsdonk, J., Murphy, J.M., Slow, E., Leavitt, B., Hayden, M., 2005. Selective degeneration and nuclear localization of mutant huntingtin in the YAC128 mouse model of Huntington disease. Hum. Mol. Genet. 3823–3835.
Van Raamsdonk, J.M., Metzler, M., Slow, E., Pearson, J., Schwab, C., Carroll, J., Graham, R.K., Leavitt, B.R., Hayden, M.R., 2007. Phenotypic abnormalities in the YAC128 mouse model of Huntington disease are penetrant on multiple genetic backgrounds and modulated by strain. Neurobiol. Dis. 26, 189–200.
Venuto, C.S., McGarry, A., Ma, Q., Kieburtz, K., 2012. Pharmacologic approaches to the treatment of Huntington's disease. Mov. Disord.: Off. J. Mov. Disord. Soc. 27, 31–41.
Vonsattel, J.P., DiFiglia, M., 1998. Huntington disease. J. Neuropathol. Exp. Neurol. 57, 369–384.
Walker, F.O., 2007. Huntington's disease. Semin. Neurol. 27, 143–150.
Wang, C.E., Tydlacka, S., Orr, A.L., Yang, S.H., Graham, R.K., Hayden, M.R., Li, S., Chan, A.W., Li, X.J., 2008. Accumulation of N-terminal mutant huntingtin in mouse and monkey models implicated as a pathogenic mechanism in Huntington's disease. Hum. Mol. Genet. 17, 2738–2751.
Wild, E.J., Tabrizi, S.J., 2017. Therapies targeting DNA and RNA in Huntington's disease. Lancet Neurol. 16, 837–847.
Wood, T.E., Yang, Z., Gray, M., Cepeda, C., Barry, J., Levine, M.S., 2018. Mutant huntingtin reduction in astrocytes slows disease progression in the BACHD conditional Huntington's disease mouse model. Hum. Mol. Genet. 28, 487–500.
Xiao, Xiao, Li, Juan, Samulski, Richard Jude, 1998. Production of high-titer recombinant adeno-associated virusvectors in the absence of helper adenovirus. J. Virol. 2224–2232.
Yan, S., Tu, Z., Liu, Z., Fan, N., Yang, H., Yang, S., Yang, W., Zhao, Y., Ouyang, Z., Lai, C., Yang, H., Li, L., Liu, Q., Shi, H., Xu, G., Zhao, H., Wei, H., Pei, Z., Li, S., Lai, L., Li, X.-J., 2018. A huntingtin knockin pig model recapitulates features of selective neurodegeneration in Huntington's disease. Cell 173 (989-1002.e1013).